Solvent free esterification of benzyl alcohol over zirconia, vanadia and ceria supported on hierarchical MFI (Mobil Five) zeolite

Mithun Nandi
Department of Chemistry, Pandit Deendayal Upadhyaya Adarsh Mahavidyalaya, Eraligool, Karimganj, Assam

Abstract - Hierarchical MFI zeolite was prepared by simple and economic alkali treatment from a sample of MFI with Si/Al molar ratio 100 which was synthesized by hydrothermal technique using green protocol. The catalytic activity of zirconia, ceria and vanadia loaded onto hierarchical MFI has been tested for benzylalcohol esterification by acetic acid. A green protocol for the esterification reaction was followed avoiding the use of any solvent. Ceria loaded sample was found to be most suitable catalyst for the reaction providing 76% conversion of alcohol and 100% selectivity for the ester. The kinetics of the reaction was also monitored for each catalysts. The reaction in all the cases follows first order kinetics with maximum rate constant of 5.19 x10^{-3} s^{-1} for the ceria supported catalyst.

Keywords - MFI ; Desilication ; hierarchical MFI ; Williamson and Hall plot ; Esterification

Graphical abstract

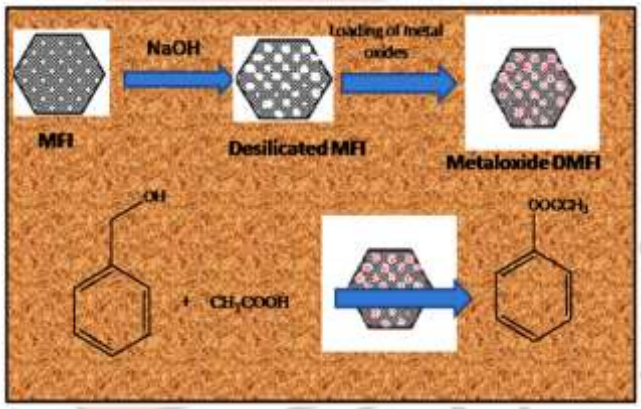

Highlights

- Hierarchical MFI was prepared by simple alkali treatment of parent MFI .
- Loading of zirconia, ceria and vanadia was carried out by impregnation technique.
- Williamson and Hall plot was employed to determine the crystallite size of the samples.
- Ceria supported catalyst was found to be more effective for benzylalcohol by acetic acid
- The kinetics study shows highest rate constant for the ceria loaded sample.

1. INTRODUCTION

Pore size engineering of zeolite is a very important tool that modifies the activity of the zeolite. Zeolites are hydrated, crystalline, microporous aluminosilicates based on a rigid 3 dimensional framework with well defined cavities and channels [1-4]. MFI represents a class of high siliceous zeolite that exhibit excellent thermal and hydrothermal stability, well designed pore and exceptional catalytic properties [5,6]. Catalysis research focussed on MFI is due to its promising performance in synfuel production [7-9], isomerisation and various hydrocarbon transformations [10-14]. In spite of being one of the most potential catalysts, the microporous nature of MFI may impose restriction on the reaction rate due to significant diffusion limitations [15-18]. This led, in recent years, to research in pore architecture engineering to develop multistructured MFI [19]. This is also because of the fact that ordered mesoporous materials such as M41S discovered in the early nineties could not decipher for some specific properties unique for MFI. The catalytic performance of mesoporous materials are also limited by their relatively poor thermal stability. The promising properties of hierarchical MFI i.e combining network of micro and mesopores have sparked intense effort to transfer fluids from active sites located mostly in the pores [20-24]. The hierarchical MFI retains strong acidity [25,26] high thermal stability and exhibits higher surface area and large pores [27,28]. The Si/Al molar ratio is an important factor for introduction of mesoporosity. Several workers have developed different techniques to overcome this limitation among which

the most simple and cost-effective post-synthesis treatment is alkali treatment [29,30] termed as desilication. The traditional post-treatment of MFI in steam or acidic medium though induces limited mesoporosity in MFI-type zeolites yet impacts directly on the acidic properties due to depletion of Bronsted acidity [31,32]. Modification of many zeolites such as MOR [33], AST [34], IFR [35], FER [36], STF [37], TON [38], FAU [39], CHA [40], MWW [41], BEA [43] by alkali treatment had been reported. Apart from NaOH, other organic and inorganic bases such as LiOH, KOH, Na_2CO_3 ,TMAOH, TPAOH and TBAOH have been used by several workers for desilication [43-45]. Our hypothesis is that these modified pores will well accommodate the active sites within them and will enhance the catalytic activities. To the best of our knowledge M. Pimsuta and co-workers [46] have used iron loaded desilicated MFI for hydroxylation of phenol. Zhou *et al* have synthesized desilicated LaZSM-5 [47] by treatment with NaOH and ion-exchange with La^{3+} under microwave irradiation in sequence for catalytic degradation of LDPE. Karen Thrane Leth *et al* found quiet satisfactory result for ethane dehydrogenation using gallium incorporated desilicated MFI [48]. Esterification reactions of carboxylic acids and alcohols are fundamental organic reactions. These reactions take place even without the use of catalyst but are very slow. Hence an highly efficient catalyst is of high demand for such reactions. Esterification rate can be enhanced by both homogenous and heterogenous acid catalysts. Typical homogenous catalyst used are HCl, H_2SO_4, HF, $ClSO_2OH$ etc [49]. A number of post reaction problems such as removal of catalyst from the reaction mixture, remains of trace amount of acid in the product even after washing. In addition it may lead to neutralization problem giving high acid number to the product. These difficulties seems to be overcomed by the use of heterogeneous catalyst that can even reduce pollution related problems. Heterogeneous catalysts such as ion-exchanged resin [50], HZSM-5, HY zeolite [51], MCM-41 [52], zirconia, alumina, silica and their sulphate, phosphate and borate modified forms have been reported to be active in esterifications [53,54]. Benzyl acetate is an important compound for perfumery, food, and chemical industries. It has a pleasant sweet aroma reminiscent of jasmine. Bhatia and his group have reported the use of Amberlyst–15 as heterogenous catalyst for the benzyl alcohol and acetic acid esterification [55]. There are also reports of carrying out the same reaction with SO_3-H functionalized ionic liquids. Silicotungstic acid/zirconia supported SBA-15 have also been tested by Sawant and co-workers [56] for the esterification of benzyl alcohol with acetic acid. The use of different zeolites such as unhierarchical Na-Y, Na-β, ZSM-5, H-ZSM-5 have also been reported in this reaction [57,58]. Considering the industrial importance of the benzyl alcohol esterification reaction and the potential application of heterogenous catalysts we tried to design some hierarchical MFI zeolite based catalyst. In this present work we have reported the catalytic properties and activities of zirconia , ceria and vanadia supported desilicated and (hence hierarchical) MFI in the synthesis of benzyl acetate and optimise the reaction conditions to get good yield of product. The kinetics of the reaction have also been worked out. A green protocol was attempted avoiding the use of any solvent during synthesis of zeolite and also in the reaction.

2. Experimental

2.1. Synthesis of MFI Zeolite

MFI with silica to alumina ratio (SAR) of 100 was synthesized using sodium aluminate (Kemphasol), fumed Silica (sigma), tetrapropylammoniun bromide (Lancaster), sodium hydroxide (Merck) and de-ionised water. A two step novel procedure previously reported from our group [59] was followed. In the first step 0.2680 g NaOH was dissolved in calculated amount of deionised water in a polyethylene beaker and set in stirring in a mechanical stirrer. 2.0126 g of tetrapropylammoniun bromide was added to it in small lots followed by 5.1790 g fumed silica . The stirring was continued for 1hr to get Gel A. In the second step Gel B is obtained by dissolving 1.4612 g NaOH in a definite amount of water followed by 14.821 g of fumed silica and 0.5495 g sodium aluminate and stirred again for an hour. The final gel obtained by stirring gel A and gel B together for another one hour was then autoclaved in a Teflon - lined stainless steel vessel maintained at 473 K inside an oven for 17 h. The autoclave was then quenched and the resultant solid product was separated from mother liquor by filtration. The product was washed several times using de-ionised water and dried at room temperature overnight and and then at 383 K and finally calcined at 750 K for 6 h to get the sodium form of MFI. The parent form of MFI is designated as PA.

2.2. Preparation of desilicated MFI sample

Modification was carried out by simple alkali treatment using NaOH. Calcined MFI (2g) was added to 150 mL of a preheated (343 K) 0.5 M NaOH solution taken in polyethylene beaker placed in a water bath and stirred constantly at that temperature for 60 min. The beaker was then immediately placed in an ice-bath to restrict further reaction. The product was filtered using Whatman filter paper (no. 40) and washed several times until all the alkali removed. The modified MFI was dried overnight at room temperature and then at 383 K for 6 h. The alkali treated MFI was designated as DS.

2.3. Impregnation of metal oxide on DS

Metal oxides zirconia, ceria and vanadia were dispersed on desilicated MFI sample (designated DS) following the impregnation technique. The precursors for zirconia , ceria and vanadia were zirconyl nitrate, ceric ammonium nitrate and vanadium acetylacetonate. Calculated amount (0.058 g, 0.098 g, 0.174 g) of Zr, Ce and V complexes respectively were dissolved in minimum amount of ethanol separately. These solutions were added separately to 1 g of DS in each case, stirred vigorously for 4 h and evaporated to dryness in air. The samples were then dried at 383 K for 6 h and finally activated by calcining for 6h at 753 K to get metal oxide loaded samples. The samples are designated as ZrDS, CeDS and VDS for zirconia, ceria and vanadia loaded MFI samples respectively.

2.4. Catalytic esterification of benzylalcohol and acetic acid

Different molar ratios of benzyl alcohol (BA) and acetic acid (AA) were taken in a 50 mL round bottomed flask followed by addition of specific amount of the catalysts. Before use all the catalysts were pretreated by heating at 383 K for 2 h. The total volume of reactants for each reaction was kept fixed at 5 mL. The reaction mixture was refluxed at different temperatures for the desired time period. The reaction mixture was withdrawn at different intervals of time and analysed by Gas

Chromatography (Bruker 430 GC) fitted with WCOT fused silica 30 m × 0.32 mm column. The conversion and selectivity were determined from the gas chromatography data using following equations,

$$\% \text{ BA conversion} = [(\text{Mole BA}_{inlet} - \text{Mole BA}_{outlet})/\text{Mole BA}_{inlet}] \times 100 \ldots (1)$$

$$\% \text{ Selectivity for benzyl acetate (BAc)} = [\text{Mole of BAc/Total mole of all products}] \times 100 \ldots (2)$$

2.5. Characterization of catalysts

The prepared catalysts were first analysed by X-ray diffraction technique. Powder X-ray diffraction patterns were recorded on a Bruker D-8 Advance X-ray Diffractometer operated at 40 kV and 40 mA using Cu K_α radiation of wavelength 0.15418 nm to determine the structure, Crystallite size. The XRD data were collected in 2θ range 5-50°(step size 0.05° and step time 0.5 s). IR spectra were recorded on KBr discs in a Perkin Elmer RX1 spectrophotometer in the mid-IR range of 1500 – 450 cm^{-1} . The surface morphology of the samples were studied by a Hitachi, S-3600N Scanning Electron Microscope. Hitachi 4100 spectrometer equipped with a diffuse reflectance attachment was used to record the diffuse reflectance UV-vis spectra of the solid catalysts in the range 200–800 nm. Transmission electron microscopy (TEM) pictures were recorded on a JEOL 2011 electron microscope. The thermal stability of all the catalysts were studied by thermal gravimetric analysis technique using Mettler Toledo TGA/DSC 1, STAR^e System Analyser in the temperature range 313-1173 K applying a heating rate of 10 min^{-1} under a nitrogen gas atmosphere. XRF spectra were recorded on an PANalytical Axios DY840 instrument. The surface area and pore size measurement were done in Micromeritics Tristar surface area and porosity analyzer.

3. Results and discussions

3.1. X-ray powder diffraction

The X-ray powder diffraction patterns of the parent and desilicated MFI are shown in Fig. 1 and those of metal oxide loaded samples ZrDS, CeDS and VDS are shown in Fig. 2. The characteristic peaks in Fig. 1 at 2θ = 7.98º**,** 23.32º and 26.86º corresponding (*101*), (*501*) and (*600*) indices of MFI respectively confirm the formation of pure phase of MFI zeolite. Alkali treatment of MFI zeolite with lower concentration of NaOH for short period of time cannot damage the basic structure of the zeolite [60]. XRD studies of the desilicated sample in the present study (Fig. 1b) reveal that the intensity of (*101*) and (*501*) planes decreases whereas that of (*600*) plane increases. The change in intensity may be due to removal of silicon from the framework without destruction of the lattice supporting the long range ordering. Loading of zirconia, ceria and vanadia decreases the intensity of all the characteristic peaks. In Fig. 2a the slight line broadening at 2θ = 30º and appearance of peak at 2θ = 50º may correspond to tetragonal phase of zirconia (Powder Diffraction file #37 -1484) loaded sample (sample ZrDS). Elshazly et al. also reported that only above 973K the monoclinic phase of zirconia appears [61]. Ceria loaded MFI (sample CeDS) in Fig. 2b shows a slight broadening of the signal at 2θ = 28° which corresponds to (*111*) plane of fcc ceria and confirmed from the JCPDS file for ceria (JCPDS 34-394). The increase in the intensity and broadening of signal at 2θ = 21º in Fig.2.c corresponds to (*001*) plane of orthorhombic V_2O_5 confirmed from JCPDS Card no.73-0514.

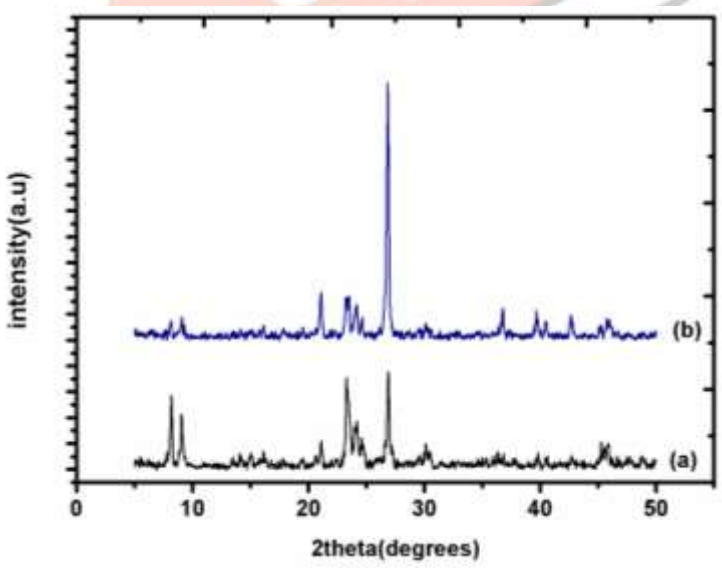

Fig.1. XRD pattern of (a) PA (b) DS

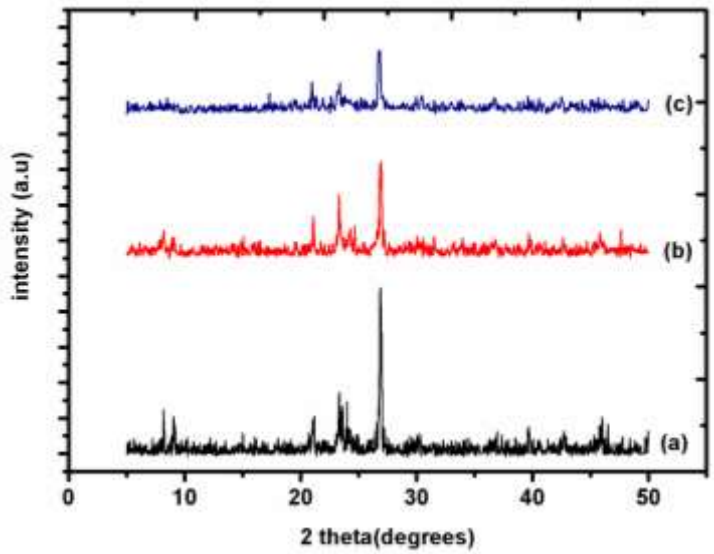

Fig.2. XRD of pattern of (a) ZrDS (b) CeDS (c) VDS

Usually average crystallite size is measured using following scherrer equation. We determined the crystallite size by simplified equation in the Lorentzian peak shape using Williamson and Hall method (Fig. 3) for deconvolating size and strain broadening

$$\beta \cos\theta = \frac{K\lambda}{D} + 4\varepsilon sin\theta$$

where, D is average crystallite size, K is a dimensionless shape factor with a value close to unity, λ is the wavelength of the X-ray, β is the line broadening at half the maximum intensity (FWHM) in radian, θ is Bragg angle in radian and ε is the average strain. The crystallite size from the Williamson –Hall plot is summarized in Table 1.

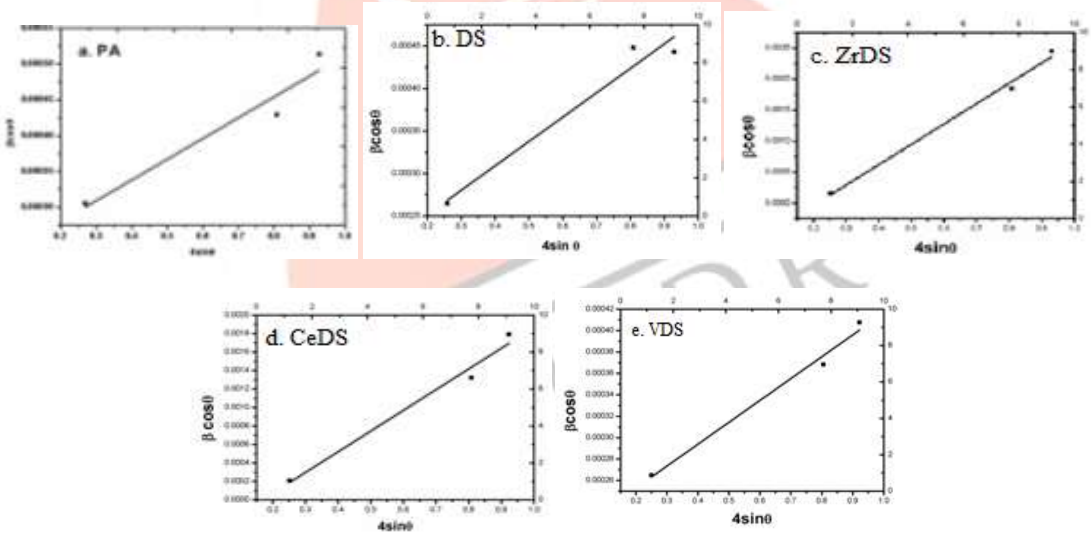

Fig.3. Williamson-Hall plot for (a) PA (b) DS (c) ZrDS (d) CeDS (e) VDS

Table 1

Crystallite size and crystallinity from XRD analysis

Entry	Sample	Intercept	Slope	Crystallite size(μm)	R^2	$(\%C)_{501}$from XRD
1	PA	2.2225 E-4	2.89E-4	0.626	0.88277	96.7

2	DS	1.94286 E-4	2.86E-4	0.713	0.92602	92.5
3	CeDS	3.75027 E-4	2.24E-3	0.369	0.96556	91.8
4	ZrDS	6.93527 E-4	3.28E-3	0.299	0.98439	74.5
5	VDS	2.12213 E-4	2.04E-4	0.653	0.97761	86.3

3.2. X-ray Fluorescence(XRF) Spectroscopy

XRF study gives information about the elemental make up of various samples. Since the samples are in powdered form, so prior to analysis they are grinned well to minimise the scatter effect due to particle size. Fig. 4 shows the XRF spectra of the parent and alkali treated MFI. The most intense peak at $2\theta = 109^{\circ}$ is assigned as SiKα. Calculation shows the removal of 17% Si from parent MFI on alkali treatment for 60 min.

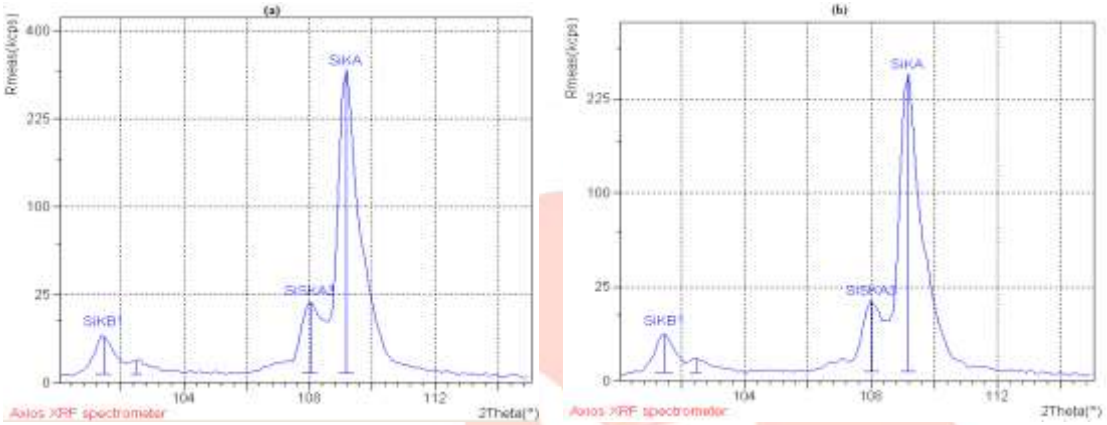

Fig. 4. XRF patterns of (a) PA (b) DS

3.3. Infrared spectroscopy

Fig. 5 illustrates the FTIR spectra of parent and modified MFI samples. The peaks at around 450, 545, 1084, 1225 cm^{-1} are characteristics peaks for MFI zeolite [62,63]. All the samples illustrates characteristics bands between 400cm^{-1} and 1250cm^{-1} (Table 2). The band at 1084 cm^{-1} is assigned to the internal asymmetric stretching of Si-O-Si or Si-O Al bonds [64]. The frequency bands at 787, 547, 450 and 1230 cm^{-1} correspond to external symmetric stretching, double ring vibration, T-O-T bending and external asymmetric stretch respectively. The slight shift in frequency and broadening of the peaks may be in response to the modification of the parent MFI.

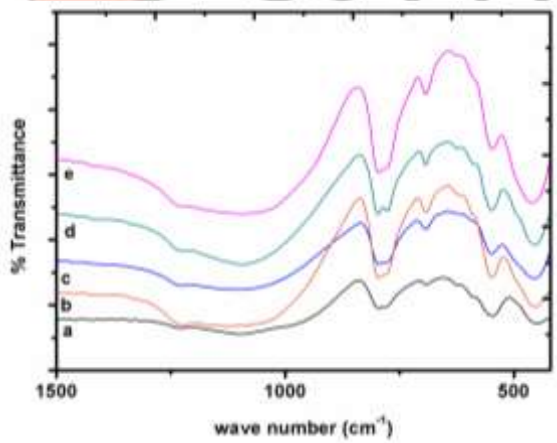

Fig. 5. FT-IR spectra of (a) PA (b) DS (c) ZrDS (d) CeDS (e) VDS

Table 2

Infrared band position of parent and modified MFI

	wave number (cm^{-1})				
Samples	Internal asymmetric stretch	External symmetric stretch	Double ring vibration	T-O bending	External asymmetric stretch

PA	1084.57	787.01	547.05	449.44	1229.03
DS	1121.70	786.10	548.49	450.46	1225.03
ZrDS	1112.41	786.12	549.94	449.44	1233.33
CeDS	1093.85	786.11	548.99	456.96	1225.53
VDS	1112.42	787.01	547.05	456.96	1232.31

3.4. UV-vis diffused reflectance spectroscopy

The UV-vis DR spectra of, ZrDS , CeDS and VDS are shown in Fig. 6. The UV-vis DR spectra of CeDS (Fig. 6b) show a single broad absorption at 310 nm suggesting $Ce^{4+} \leftarrow O^{2-}$ charge transfer (tetrahedral Ce^{4+}) and the longer wavelength at 405 nm account for CeO_2 for hexa coordinated Ce^{4+} [65] . The spectra of sample VDS exhibit two absorption bands in the wavelength range of 240-350 nm (Fig. 6c). The broad and strong band in the range 280-350 nm indicates the $V^{5+} \leftarrow O^{2-}$ charge transfer suggesting presence of tetrahedral vanadium species [66-67] , a shoulder at 240 nm corresponding to V^{4+} charge transfer band of VO^{2+} species and at around 400 nm assigned to V^{5+} in octahedral environment [68]. In Fig. 6a the absorbance in the range 290 – 330 nm can be attributed to the presence of low coordination surface tetragonal ZrO_2 exhibiting $Zr^{4+} \leftarrow O^{2-}$ transition [69,70].

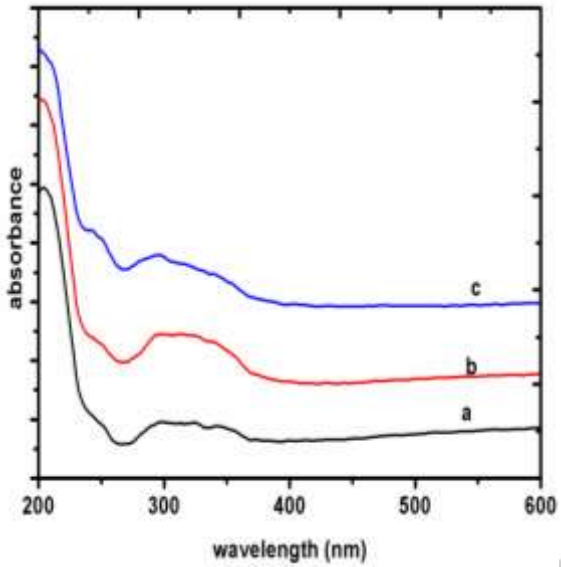

Fig.6. UV-vis DRS of (a) ZrDS (b) CeDS (c) VDS

3.5. Thermal gravimetric analysis

The initial weight loss up to 423 K for the parent MFI sample (Fig. 7a) resulted from desorption of water. The loss during 373 – 423 K is assigned to the desorption of occluded water. The mass loss increases in the temperature range 423 – 773 K while beyond 773 K the rate of degradation decreases. Round *et al* well documented these two phases of mass loss due to loss of four types of tetrapropylammonium (TPA^+) cations [71]. The cations that are ion-paired to crystal surface defect and that occluded in the MFI channels are lost most easily and falls in the first and second type respectively. The third type of cationic species neutralises internal framework defects and the weight loss above 773 K that neutralises the framework negative metal centres constitutes the fourth type. The desilicated sample shows weight loss at 373 K due to physically adsorbed water and the weight loss in the broad temperature range of 373–1073 K can be attributed to the decomposition of sodium hydroxide. Since the desilicated sample was calcined previously no loss of organic template is observed [72]. For uncalcined ceric ammonium nitrate loaded sample (Fig. 7e) the first breakdown continues till 383 K . The prominent breakdown in the region 383– 673 K is due to the decomposition of $Ce(IV)(NH_4)_2(NO_3)_6$ attributed to the following set of reactions passing through double valence change of cerium [73]

$Ce(IV) \rightarrow Ce(III) \rightarrow Ce(IV)$. $Ce(IV)(NH_4)_2(NO_3)_6 \rightarrow 1/3\ Ce(III)_2(NH_4)_3(NO_3)_9 + 1/3CeO_2 +$ (NH_3, NO, NO_2, O_2) (388 – 523 K)

$1/3\ Ce(III)_2(NH_4)_3(NO_3)_9 \rightarrow 2/3CeO_2 + (NH_3, NO, NO_2, O_2)$ (523 – 673 K)

The initial breakdown (below 473 K) for uncalcined zirconyl nitrate loaded sample (Fig. 7d) is due to the removal of sorbed water. The next breakdown in the range 473– 673 K can be attributed to the decomposition of nitrates [74]. The decomposition during 713 – 723 K takes place by the complete removal of nitrates and simultaneous crystallization of zirconia on zeolite surface. For the uncalcined vanadyl acetylacetonate loaded sample the breakdown near 373 K is due to the removal of adsorbed water. The second breakdown in the range 473 - 723 K could be attributed to the thermal decomposition of organic ligands from $VO(acac)_2$. The next breakdown thereafter till 873 K possibly indicated the combustion of residual organics and incipient cyystallization of V_2O_5 [75] .

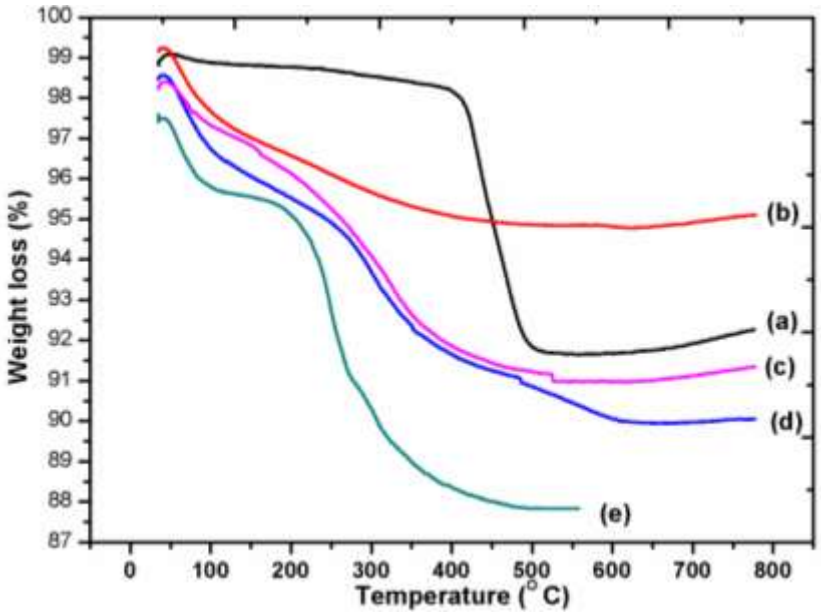

Fig. 7. TGA curves of (a) PA (b) DS (c) VDS (d) ZrDS (e) CeDS

3.6. Scanning Electron Microscopy

Fig. 8 shows the SEM images of the parent and modified MFI samples. Fig. 8a illustrates small cuboidal and hexagonal crystals of around 6μm in size for parent MFI. After alkali treatment the morphology of the MFI zeolite somewhat changed (Fig. 8b). Some cracks and faults appeared on the surface of MFI particle. Vanadia and zirconia supported samples shows some agglomeration of the particles.

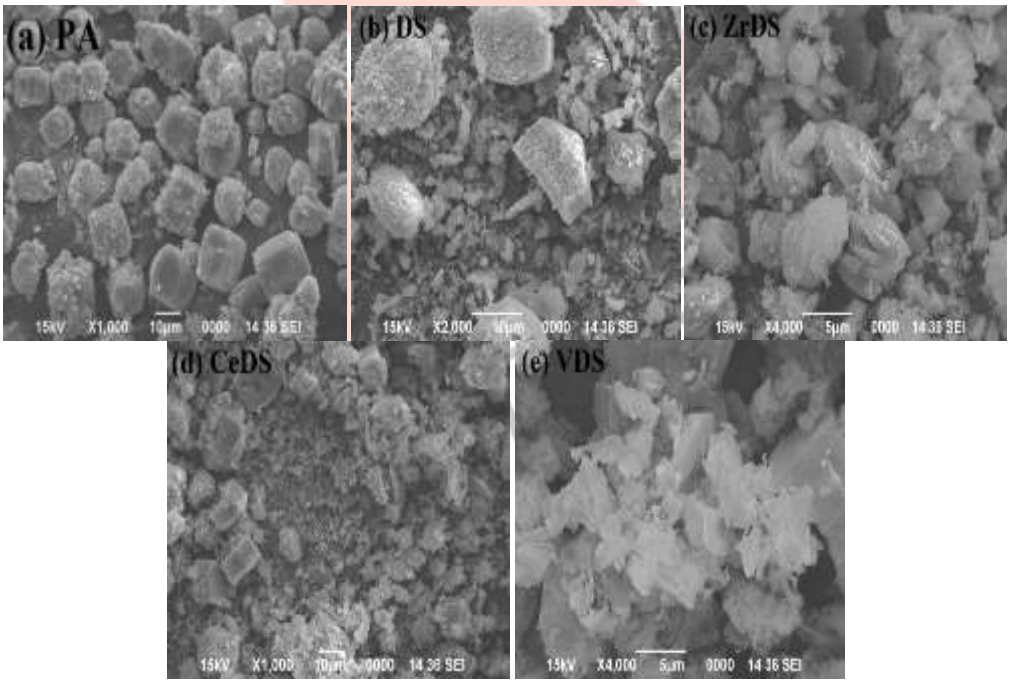

Fig. 8. SEM micrograph of (a) PA (b) DS (c) ZrDS (d) CeDS (e) VDS

3.7. Transmission Electron Microscopy

TEM images (Fig. 9) confirm the dispersion of metal oxide particles into the micro and meso pores of the desilicated MFI zeolite. The TEM images reveal the co-existence of smaller crystals due to the metal oxides supported on to the larger ones for the zeolite. Ceria impregnated (Fig. 9b) hierarchical MFI indicated the presence of a narrow range particle size distribution than in case of vanadia (Fig. 9c) and zirconia (Fig. 9a) loaded samples.

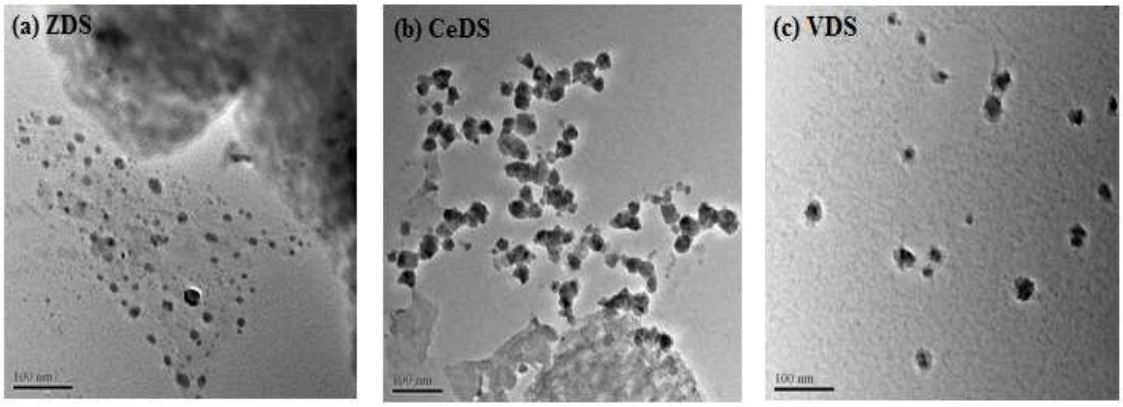

Fig.9. TEM images of (a) ZrDS (b) CeDS and (c) VDS

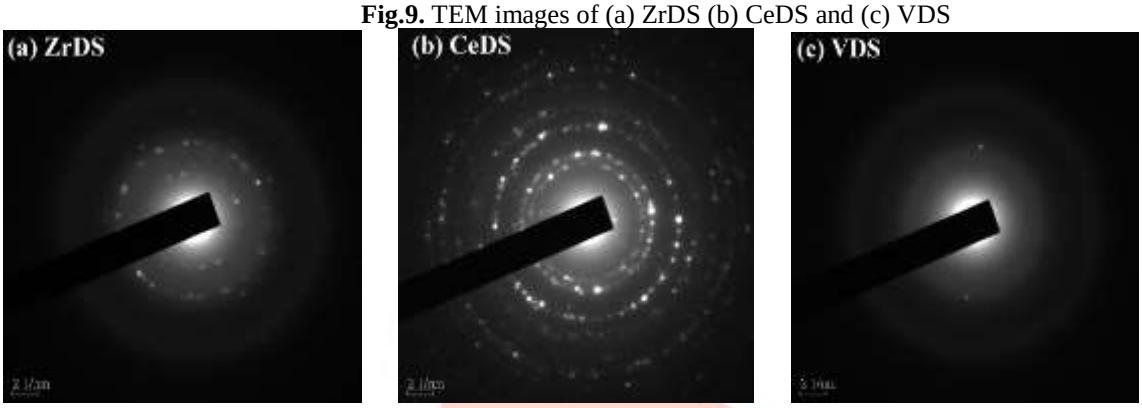

Fig.10. Selected area electron diffraction (SAED) pattern of (a) ZrDS (b) CeDS (c) VDS

The SAED is obtained by focussing the electron beam on the metal oxide particles lying on the TEM grid. It is the projection of the reciprocal lattice with lattice reflection showing as diffraction spots and each spot arising from Bragg reflection from an individual crystallite. SAED gives information about the crystallinity of a sample and more specifically about the electron diffraction pattern from a selected area. Fig. 10 shows the SAED pattern of zirconia ,ceria and vanadia supported samples respectively. The diffraction spots making rings shows polycrystalline nature for all the three samples. Supported ceria sample shows more ordered ring patterns demanding to be more crystalline and well dispersed than the other two. Moreover the most brightest diffraction spots for CeDS (Fig. 10b) also suggest its highest crystallinity among others. Vanadia loaded sample (Fig. 10c) seems to be the least crystalline among the synthesized samples. The observations are in good parity with the XRD data.

3.8. Surface area analysis

Prior to analysis surface area determination all the samples were degassed by passing a constant flow of nitrogen at 473 K for 6 h to remove any adsorbed gases. Fig. 11 depicts the nitrogen adsorption-desorption isotherm of the parent and desilicated MFI samples. The parent MFI exhibits a type1 isotherm with high up-taking at relatively low pressure indicating its microporous nature [76]. The isotherm of the alkali treated MFI (Fig. 11b) and metal oxide loaded samples (Fig. 12) shows the presence of hysteresis loop along with capillary condensation confirming the presence of mesopore structure [77] . The shapes of the isotherm are found to be of type-IV with a H3 hysteresis loop at p/p_o= ~0.45 – 0.95 indicating some amount of mesoporosity. The BET surface area (S_{BET}), average pore diameter (D_{Pore}) and limiting micropore volume (Vm_{Pore}) of all the catalysts are given in Table 3. BET surface area of the parent MFI (sample PA) was found to 396 m^2/g which increased to 439m^2/g on alkali treatment for a duration of 60 min (sample DS). The surface area of the metal oxide loaded samples decreases considerably (234.4, 280.7 and 231.6 m^2/g respectively for ZrDS, CeDS and VDS) due to pore blockage by metal oxide particles. The average pore diameter of desilicated sample was found to be 14 nm which is quiet significant in comparison to the parent one with 2.17 nm. The increase in the pore size in case of desilicated sample is due to the extraction of silicon from the MFI framework. The average pore size of the all impregnated samples decreases and found to be around 3 nm which is again due to the same reason as stated for decrease in the surface area. Dubin–Astakhov equation was used to obtain the limiting micropore volume. The micropore volume for the parent MFI is found to be 0.163cm^3/g and this volume seems to decrease for the desilicated and metal oxide loaded samples.

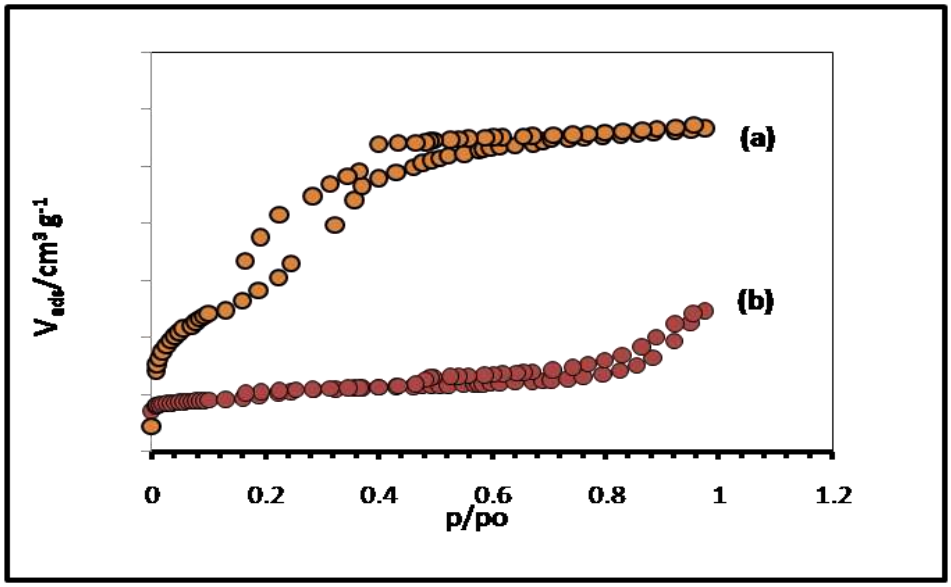

Fig. 11. N_2 adsorption – desorption isotherm of (a) PA (b) DS

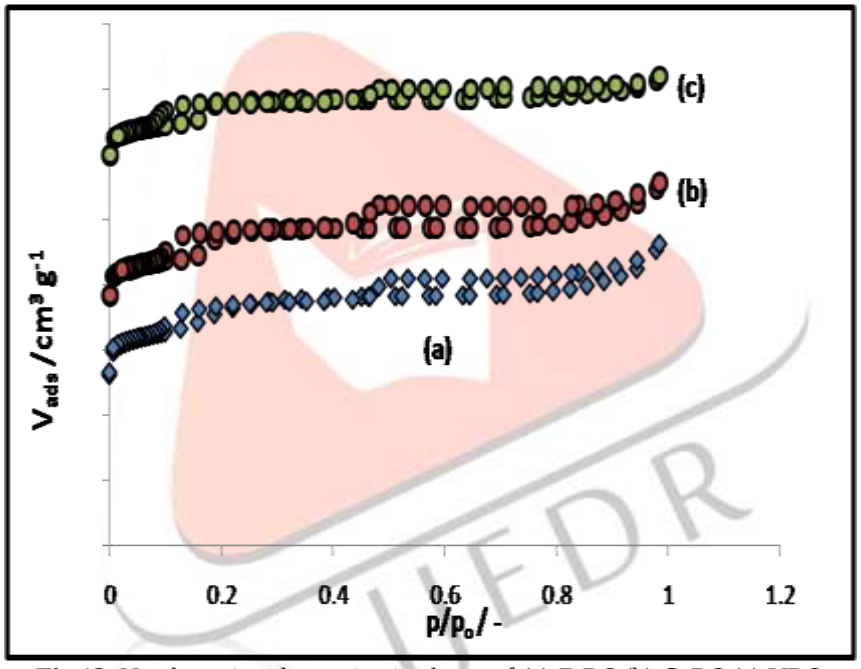

Fig.12. N_2 adsorption-desorption isotherm of (a) ZrDS (b) CeDS (c) VDS

Table 3

Surface area and porosity of parent and modified MFI samples

Entry	Samples	S_{BET} (m^2/g)	D_{Pore} (nm)	Vm_{Pore}(cm^3/g)
1	PA	396.9	2.17	0.163
2	DS	439.6	14.6	0.122
3	ZrDS	234.4	3.38	0.053
4	CeDS	280.7	3.28	0.055
5	VDS	231.6	3.15	0.040

4. Catalytic activity

All the synthesized catalysts were evaluated for well-known benzyl alcohol (BA) and acetic acid (AA) esterification reaction (Scheme 1). Reaction conditions were optimized taking DS as model catalyst to assess the effect of reaction time, temperature, mole ratio of the reactants, amount of catalyst etc. A green protocol was attempted avoiding the use of any solvent system. The reaction was monitored constantly and samples withdrawn after specific intervals of time were analysed by Gas Chromatography.

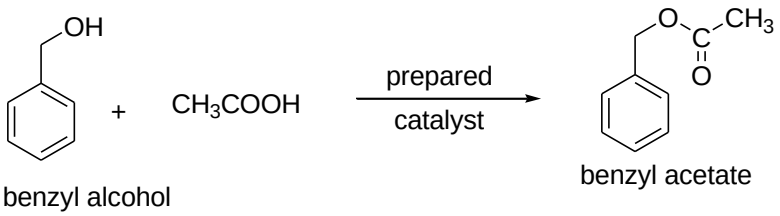

Scheme.I Esterification reaction of benzyl alcohol with acetic acid

4.1 . Effect of reaction time at temperature

Catalytic esterification of benzyl alcohol (BA) and acetic acid (AA) was studied at different temperatures (333–373 K) with 1:2 molar ratio of BA to AA with 0.2 g DS catalyst. At room temperature the conversion was negligible for a sufficiently longer time . The conversion increased from 11% to 58% in 4 h when the temperature was raised from 333 K to 373 K with benzylacetate as the only product (Fig. 14). Reaction time as a function of BA conversion is shown in Fig. 13. Initially the conversion of BA increased rapidly and gradually levelled off after 4 h. The conversion of BA at 373 K increases from 15% for first 30 min to 58% in 4 h and on proceeding further to 6 h the conversion reaches 63%. The reaction at 373 K was continued till 8 h but there was no any formation of side products.

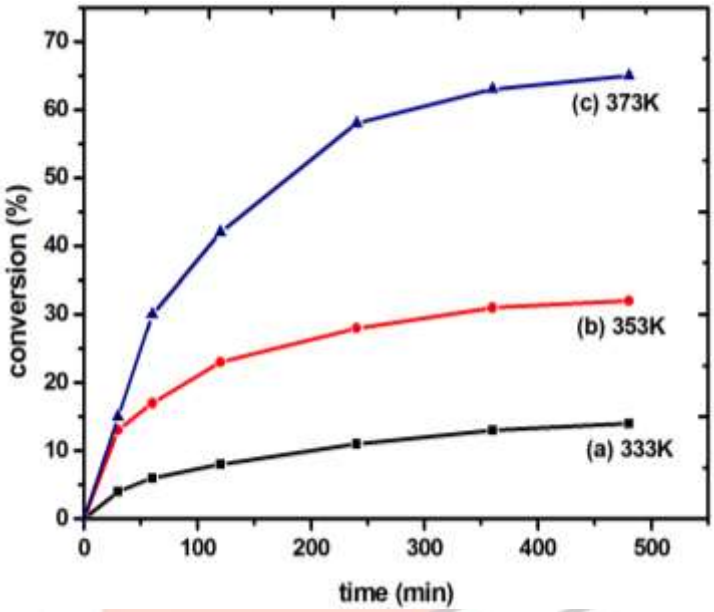

Fig. 13. Effect of reaction temperature and time (a) 333 K (b) 353 K (c) 373 K (BA : AA = 1:2, 0.2 g DS)

4.2 . Effect of Molar ratio

The reaction was carried out with BA to AA molar ratios of 1:1, 1:2 and 2:1 maintaining a total volume of 5 mL of substrates. The results are shown in Fig. 14. With 1:2 molar ratio of the reactants the conversion was found to be 58% under the mentioned rection conditions. The conversion decreased to 26% and 14 % as molar ratio changed to 1:1 and 2:1 respectively. However, the selectivity towards benzylacetate was 100% in all the cases. Hence 1:2 molar ratio of BA : AA had been taken as the optimised molar ratio for further reactions.

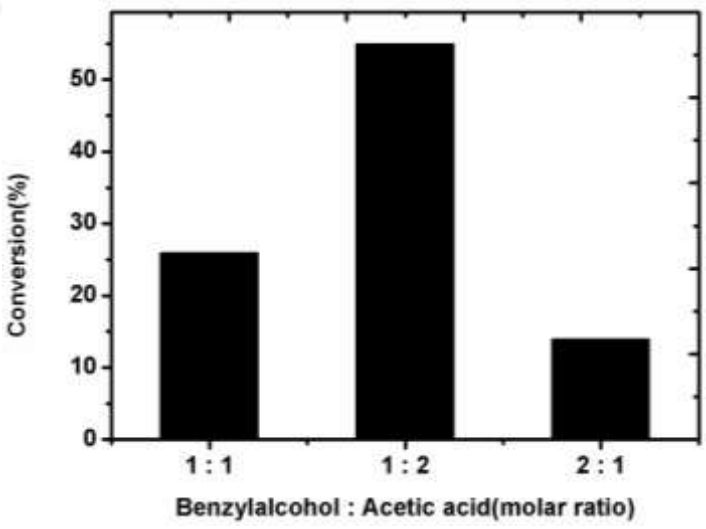

Fig. 14. Effect of molar ratio over DS catalyst time = 4 h, 0.2 g catalys

4.3 **.** *Effect of catalyst concentration*

Influence of catalyst concentration was tested by varying the DS amount from 0.05 to 0.5 g (Fig. 15) keeping the molar ratio of BA to AA 1:2 at 373 K for 4 h. The conversion increases from 46% to 58% when amount of catalyst increases from 0.05 g to 0.2 g but on further increasing the catalyst amount to 0.5 g leads to a minimal increase of 1% in the conversion of BA.

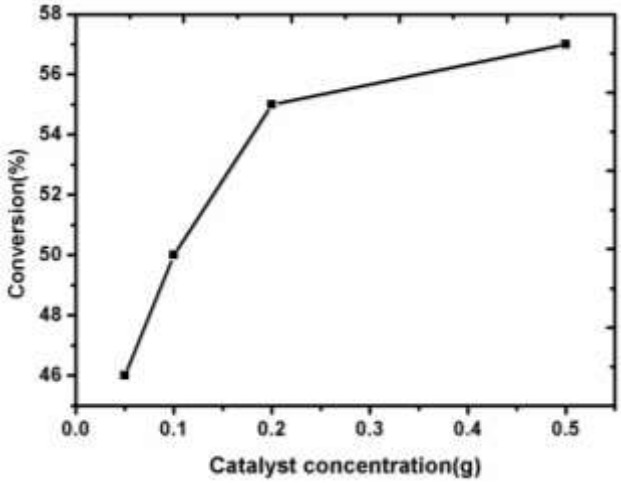

Fig. 15. Effect of catalyst concentration on conversion (BA : AA = 1 : 2, 373 K, 4 h)

4.4. Kinetics of the esterification reaction

The kinetics of the esterification reaction was carried by several workers with different solid catalysts such as zeolite HZSM-5, HY, Hß [58] anion modified zirconia, alumina and silica [53-54] silicotungstic acid/zirconia supported SBA-15 [56]. In the present study kinetics was first studied for catalyst DS in the temperature range 333-373 K. A plot of –ln (1- conversion) versus reaction time in Fig. 16 shows a linear variation indicating the reaction to be first order. This kinetics study was then compared with that of the parent MFI as shown in Fig. 17. A comparative kinetics was carried out for all other catalysts at 373 K (Fig. 18) gave linear plots which the reaction to be of first order. The rate constants for all the reactions that are directly obtained from the corresponding slopes are presented in Table 4 and 5.

Table 4
Reaction rate constant at different temperatures over DS catalyst

Catalyst	Temperature(k)	Rate constant	R^2
DS	333	5.61×10^{-4}	0.97451
	353	1.61×10^{-3}	0.91456
	373	3.61×10^{-3}	0.90599

Table 5
Comparision of reaction rate constant for all the synthesized catalysts

Temperature (K)	Catalysts	Rate constant	R^2
373	PA	2.40×10^{-3}	0.98384
	DS	3.61×10^{-3}	0.97451
	VDS	3.83×10^{-3}	0.97407
	ZrDS	4.05×10^{-3}	0.97263
	CeDS	5.19×10^{-3}	0.97751

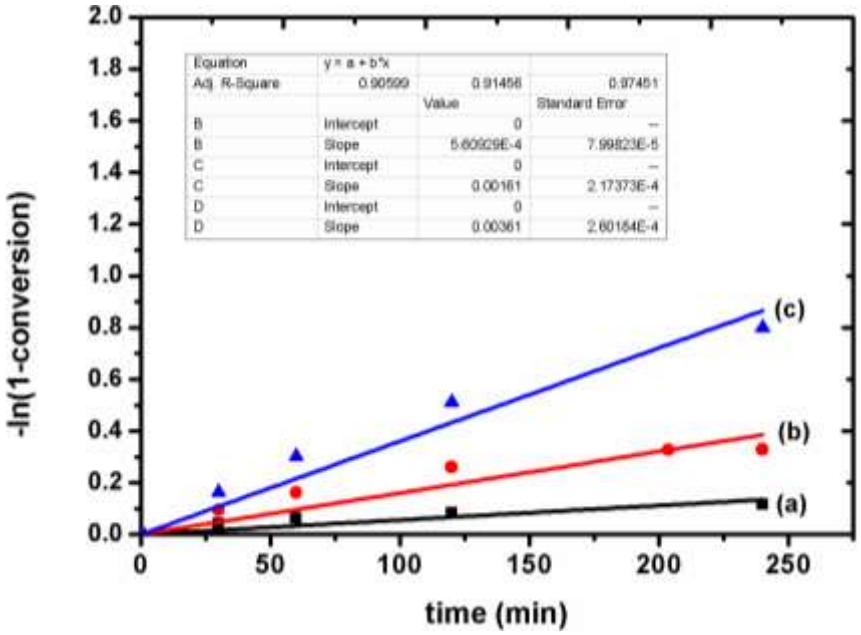

Fig. 16. First- order rate equation plot at three different temperatures
(a) 333 K (b) 353 K (c) 373 K. BA : AA = 1 : 2, 0.2 g catalyst

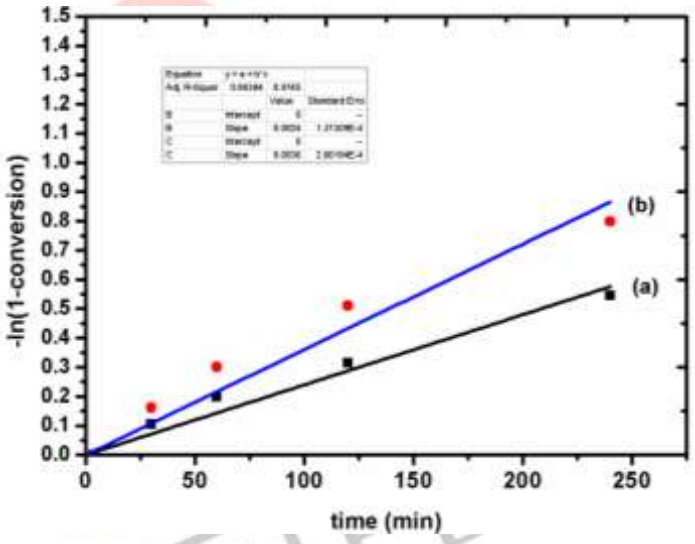

Fig. 17. First order plot for the esterification reaction over (a) PA (b) DS.
BA : AA = 1 : 2, 0.2 g catalyst, 373 K

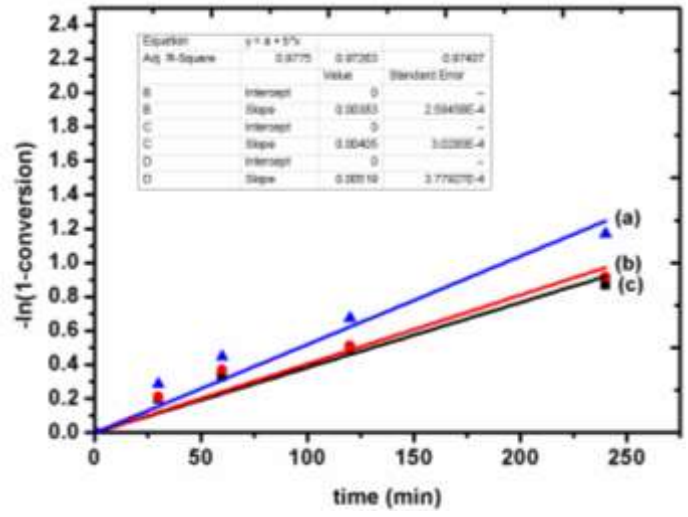

Fig. 18. Plot of the first order rate equation over (a) CeDS (b) ZrDS (c) VDS
BA : AA = 1 : 2, 0.2 g catalyst, 373 K

4.5. Comparision of the catalytic activity of the synthesized catalyst

The catalytic activity of all the synthesized catalysts were compared under the optimized conditions. Easy diffusion of substrate and product molecules to and from the active sites of zeolite surface is a prerequisite for better conversion of the substrate. In the present reaction of benzyl alcohol esterification desilicated MFI sample gave higher conversion than the parent one under any reaction conditions (Fig. 19). The reason is attributed to the enhanced surface area and pore volume of desilicated sample. If we compare the activity of parent MFI (PA) with desilicated one (DS) in the benzyl alcohol esterification reaction, we find that there were around 4 to 12% increase in the conversion for DS sample under same reaction conditions. The structure-property function relationship between creation of mesoporosity in zeolite and catalytic activity of the same was proved by various authors [36, 78-79] and we believe that the hierarchy factor definitely helps in our case also. The introduction of mesoporosity in hierarchical zeolite is coupled with a lowered micropore volume. The hierarchy factor (HF) which is defined as the

$$HF = (S_{meso}/S_{total}) \times (V_{micro}/V_{total})$$

is used to find hierarchical structure formation independent of methodology, where S_{meso} =..external surface area, S_{total} =. total surface area, V_{micro}=..micropore volume, V_{total} = total pore volume, (S_{meso} /S_{total}) is the relative mesopore surface area and (V_{micro}/V_{total}) is the relative microporosity. In the present study, HF value is found to be 0.186 and 0.232 respectively for parent and desilicated samples respectively showing clear formation of hierarchical zeolite. True value of HF value becomes clear when related to catalytic property and in our case it is proved by the result of increase of conversion of benzyl alcohol as stated above. With the optimised conditions of molar ratio (BA : AA) = 1:2 at 373 K with 0.2 g of catalyst the reaction was carried out for rest of the synthesized catalysts i.e VDS, ZrDS and CeDS. The conversions are plotted against time and shown graphically in Fig. 16. Under the similar reaction conditions in the esterification of benzyl alcohol ceria loaded sample seems to give the maximum conversion of 76% (order being PA < DS < VDS < ZrDS < CeDS) among all the synthesized catalysts. The better catalytic activity of the ceria supported sample may be due to the presence of dual sites in ceria, the acid – base and the redox sites. Loading of oxides on the surface of desilicated MFI sample had caused decrease in surface area leading to decreased pore volume and pore diameter (Table 3). However conversion of benzyl alcohol with oxide loaded MFI was found to increase indicating a prominent role of metal oxides (MO_x) in the overall conversion of BA. Based on the earlier works over loaded metaloxides [80] scheme II may be proposed for the possible reaction pathway for the esterification of benzylalcohol and acetic acid.

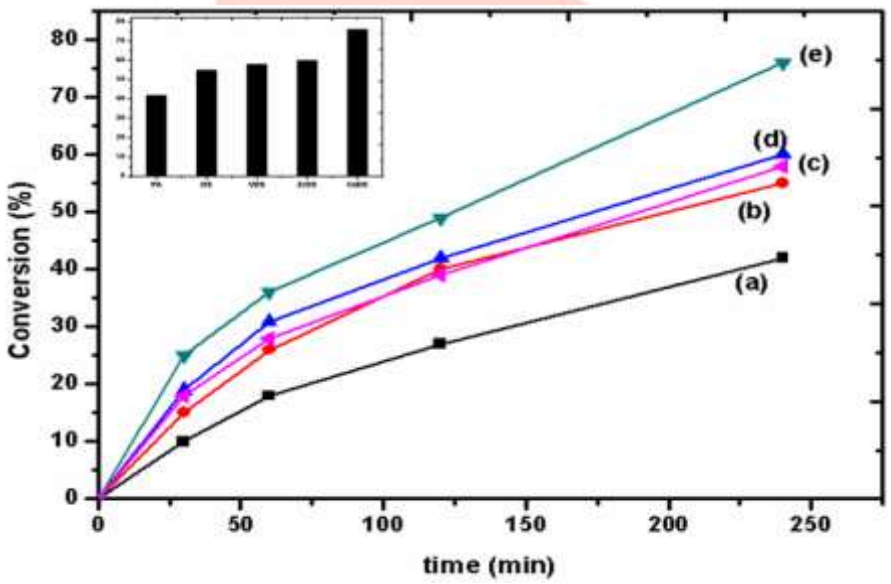

Fig. 19. Comparison of the catalytic performance of the synthesized catalysts in benzyl alcohol esterification reaction . BA : AA = 1 : 2, 373 K, 0.2 g catalyst (inset compared at 4 h)

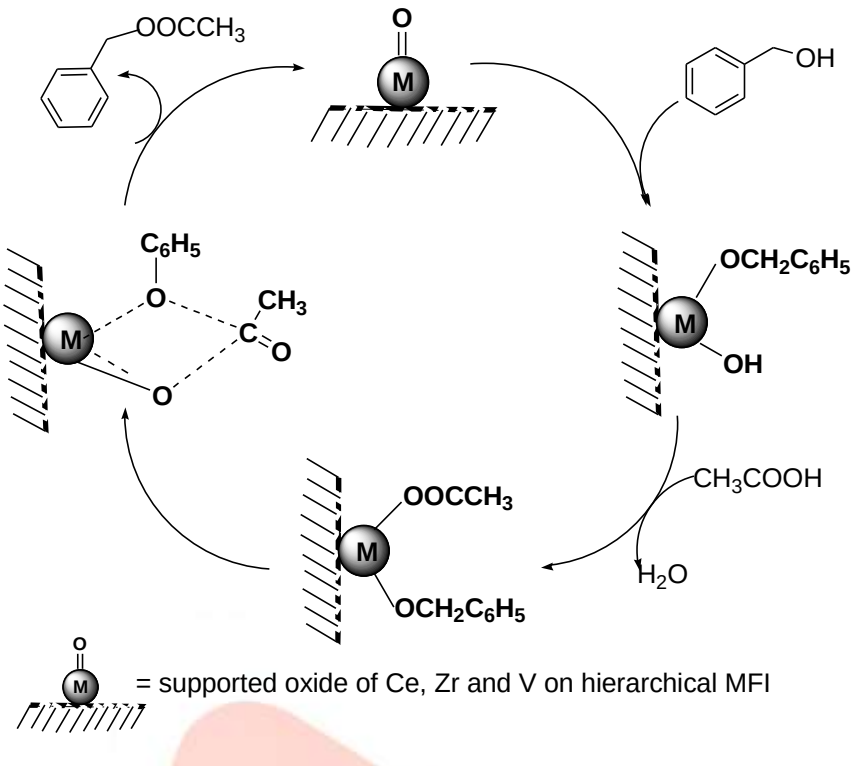

Scheme II. Proposed mechanism for the esterification of benzylalcohol and acetic acid over loaded oxides

5. Conclusion

All the catalysts demonstrated high catalytic activity for benzyl alcohol esterification reaction. Since formation of dibenzylether was not observed hence it can be inferred that most of the active sites are present inside the pores. The restricted pore size donot allow the formation of bulky dibenzylether in any of the case. The conversion shown by MFI and its desilicated form may be due to the presence of acid sites in them whereas different mechanism has been proposed for benzyl alcohol esterification using metal oxide loaded hierarchical MFI samples. Oxides of cerium, zirconium and vanadium have been successfully accommodated onto the hybrid strucyure of hierarchical MFI zeolite created through desilication without damaging the basic network of the zeolite. The crystallite size of desilicated sample has been found to increase than the parent one as evidenced from Williamson-Hall method of crystallite size determination deconvolating size and shape broadening. Crystallite size for oxide loaded samples have been found to be less except for vanadium oxide loaded MFI sample. TEM and SAED image showed best dispersion and crystallitinity for the ceria loaded sample.

Acknowledgement

The authors are grateful to UGC for providing BSR fellowship to one of the workers. The authors also acknowledge Department of Chemistry, Department of Instrumentation & USIC, Gauhati University ,CIF of NEHU and IITG for sample analysis.

References

[1] J. Cejka, H. van Bekkum, A. Corma, F. Schueth, Introduction to Zeolite Molecular Sieves, third ed., Oxford, U.K., 2007.
[2] Y.Tao, H. Kanoh, L. Abrams, K. Kaneko, Chem. Rev. 106 (2006) 896.
[3] C. Bartholomew, R.J. Farrauto, Fundamentals of industrial catalytic processes, second ed., Wiley and Sons, Hoboken, 2005.
[4] J.T. Richardson, Journal of catalysis 9 (1967) 182.
[5] D.H. Olson, G.T. Kokotailo, S.L. Lawton, J. Phys. Chem. 85 (1981) 2238.
[6] G.T. Kokotailo, S.L. Lawton, D.H. Olson, Nature 272 (1978) 437.
[7] D.A. Whan, Chem. Brit. 17 (1981) 532.
[8] Y.N. Li, S.L. Liu, S.J. Xie, L.Y. Xu, Appl. Catal. A: Gen. 360 (2009) 8.
[9] J.C. Groen, J.A. Moulijn, J. Perez-Ramirez, J. Mater. Chem. 16 (2006) 2121.
[10] L. Su, L. Liu, J. Zhuang, H. Wang, Y. Li, W. Shen, Y. Xu, X. Bao, Catal. Lett. 91(2003) 155.
[11] J.S. Jung, J.W. Park, G. Seo. Appl. Catal. A: Gen. 288 (2005 149.
[12] T.C. Tsai, S.B. Liu, I. Wang, Appl. Catal.A: Gen. 18 (1999) 355.
[13] V.S. Nayak, L. Riekert, Appl. Catal. 23 (1986) 403.
[14] X. Chang, Y. Li, Z. Zeng, Ind. & Eng. Chem. Res. 31 (1992) 187.
[15] M. Hartmann, Angew. Chem. Int. Ed. 43 (2004) 5880.
[16] J. Perez-Ramirez, C.H. Christensen, K. Egeblad, C.H. Christensen, J.C. Groen, Chem. Soc. Rev.37 (2008) 2530.
[17] Y. Tao, H. Kanoh, K. Kaneko, Langmuir 21 (2005) 504.
[18] K. Egeblad, C.H. Christensen, M. Kustova, C.H.Christensen, Chem. Mater. 20 (2008) 946.

[19] H. van Bekkum, E.M. Flanigen, J. Jansen, Introduction to zeolite science and practice 58 (1991) 19.
[20] J. Pe´rez-Ramı´rez, C. H. Christensen, K. Egeblad, C. H. Christensen, J. C. Groen, Chem. Soc. Rev. 37 (2008) 2530.
[21] J.C. Groen, T. Bach, U. Ziese, A.M. Paulaime-van Donk, K.P. de Jong, J.A. Moulijn, J. Perez-Ramirez, J. A.m. Chem. Soc. 127 (2005)10792.
[22] J.C. Groen, W. Zhu, S. Brouwer, S.J. Huynink, F. Kapteijn, J.A. Moulijn, J. Perez-Ramirez, J. A.m. Chem. Soc.129 (2007) 355
[23] L. Zhao, B. Shen, J. Gao, C. Xu, J. Catal. 258 (2008) 228.
[24] X. Li, R. Prins, J.A. van Bokhoven, J. Catal. 262 (2009) 257.
[25] X. Wei, P.G. Smirniotis, Micropor. Mesopor. Mater. 97 (2006) 97.
[26] D. Verboekend, S. Mitchell, M. Milina, J.C. Groen, J. Perez-Ramírez, J. Phys. Chem. C 115 (2011) 14193.
[27] C. Fernandez, I. Stan, J.P. Gilson, K. Thomas, A.Vicente, A. Bonilla, J. Perez-Ramirez, Chem. Eur. J. 16 (2010) 6224.
[28] M. Ogura, S. Shinomiya, J. Tateno, Y. Nara, E.Kikuchi, M.Matsukata, Chem. Lett. 8 (2000) 882.
[29] J.C. Groen, L.A.A. Peffer, J.A. Moulijn, J. Perez-Ramirez, Microporou Mesoporous Mater. 69 (2004) 29.
[30] M. Ogura, S. Shinomiya, J. Tateno, Y. Nara, M. Nomura, E. Kikuchi, M. Matsukata, Appl. Catal. A 219 (2001) 33.
[31] J. Peerez-Ramirez, S. Mitchell, D. Verboekend, M. Milina, N.L. Michels, F. Krumeich, N. Marti, M. Erdmann, ChemCatChem 3 (2011) 1731.
[32] J. Scherzer, ACS Symp. Ser. 248 (1984) 157.
[33] J.L. Motz, H. Heinichen, W.F. Holderich, J. Mol. Catal. A: Chem. 136 (1998) 175.
[34] J.C. Groen, T. Sano, J.A. Moulijn, J. Perez-Ramirez, J. Catal. 251 (2007) 21.
[35] J. Perez-Ramirez, S. Abello, L.A.Villaescusa, A. Bonilla, Angew. Chem. Int. Ed. 47 (2008) 7913.
[36] D. Verboekend, J.C. Groen, J. Perez-Ramirez, Adv. Funct. Mater.20 (2010) 1441.
[37] A. Bonilla, D. Baudouin, J. Perez-Ramirez, J. Catal. 265 (2009) 170.
[38] Z. Musilova-Pavlackova, S.I. Zones, J. Cejka, Top. Catal. 53 (2010) 273.
[39] D. Verboekend, A.M. Chabaneix, K. Thomas, J.P. Gilson, J. Perez-Ramírez, J.Cryst Eng Comm 13 (2011) 3408 .
[40] K.P. de Jong, J. Zecevic, H. Friedrich, P.E. de Jongh, M. Bulut, S. van Donk, R. Kenmogne, A. Finiels, V. Hulea, F. Fajula, Angew. Chem. Int. Ed. 49 (2010) 10074.
[41] L. Sommer, D. Mores, S. Svelle, M. Stocker, B.M. Weckhuysen, U. Olsbye, Microporous Mesoporous Mater. 132 (2010) 384.
[42] Y. Mokrzycki, B. Sulikowski, Z. Olejniczak, Catal. Lett.127 (2009) 296.
[43] J.C. Groen, S. Abello, L.A. Villaescusa, J. Perez-Ramírez, Microporous Mesoporous Mater.114 (2008) 88.
[44] J.C. Groen, J.A. Moulijn, J. Pérez-Ramírez, Ind. Eng. Chem. Res. 46 (2007) 4193.
[45] Q. Zhou, Y.Z. Wang, C. Tang, Y.-H. Zhang, Polym. Degrad. Stab. 80 (2003) 23.
[46] M.S. Holm, M.K. Hansen, C.H. Christensen, Eur. J. Inorg. Chem. 9 (2009) 1194.
[47] M. Pimsuta, A. Neramittagapong, S. Prayoonpokarach, J. Wittayakun, International Journal of Chemical Engineering and Applications 3 (2012) 86.
[48] K.T. Leth, A.K. Rovik , M.S. Holm, M. Brorson ,H.J. Jakobsen , J. Skibsted , C.H. Christensen, Applied Catalysis A: General 348 (2008) 257 .
[49] T. Okuhara, N. Mizuno, M. Misono, Adv. Catal. 41 (1996) 113.
[50] G.A. Olah, T. Keumi , D. Meidar , Synthesis 12 (1978) 929.
[51] Y. Ma, Q.L. Wang, H. Yan, X. Ji, Q. Qiu, Applied Catalysis A: General 139 (1996) 51.
[52] R. Kester, B. Linden, E. Poels, A. Blick, J Catal 204 (2001) 333.
[53] K. Tanabe , M. Misono, Y. Ono, H. Hattori, Stud Surf Sci Catal 51 (1989) 285.
[54] D. Souza , N. Nagaraju, Indian Journal of Chemical Technology 13 (2006) 605.
[55] R. Roy , S. Bhatia , Journal of Chemical Technology and Biotechnology, 37 (2007) 1.
[56] P. Dhanashri, P. Sawant, A. Vinu, J. Justus , P. Srinivasu , S.B. Halligudi , Journal of Molecular Catalysis A: Chemical 276 (2007) 150.
[57] K.R. Sharath, S. Vijayashree, N. Nagaraju, Indian Journal of Chemical Technology 8 (2001) 362.
[58] S.R. Kirumakki, N. Nagaraju, S. Narayanan, Applied Catalysis A: General 273 (2004) 1.
[59] B. Kalita, A.K. Talukdar, Mater. Res. Bull. 44 (2009) 254.
[60] R. Caicedo–Realpe, J. Perez-Ramirez, Microporous and Mesoporous materials 128 (2010) 91.
[61] E.S. Elshazly , O.A.A. Abdelal , International Journal of Metallurgical Engineering 1 (2012) 130 .
[62] P.A. Jacobs, H.K. Beyer, J.Valyon, Zeolites, 1 (1981) 161.
[63] R.M. Mohamed, H.M. Aly, M.F. El-Shahat, and I. A. Ibrahim, Microporous Mesoporous Mater 79 (2005) 7.
[64] V. Mohan, C. Raghavendra, C.V. Pramod, B. D. Raju , K. S. R. Rao, RSC Adv. 4 (2014) 9660.
[65] A. Bensalem, J.C. Muller, F.B. Verduraz, J. Chem. Soc Faraday Trans 88 (1992) 153.
[66] H. Ronde, J.G. Snijders, Chem. Phys. Lett. 50 (1977) 282.
[67] S.H. Jhung, Y.S. Uh, H. Chon, Appl. Catal. 62 (1990) 61.
[68] G. Centi, S. Perathoner, F.Trifiro, A. Aboukais, C.F.Aissi, M.J.Guelton, J. Phys. Chem. 96 (1992) 2617.
[69] G. Ranga Rao, H.R. Sahu, Proc. Indian Acad. Sci.Chem. Sci. 113 (2001) 651.
[70] C.R. Aita, C. Kwok, J. Am. Ceram. Soc. 73 (1990) 3209.
[71] C.I. Round, C.D. Williams, K. Latham, C.V.A. Duke , Journal of Thermal Analysis and Calorimetry 63 (2001) 329.
[72] R. Caicedo-Realpe , J. Perez-Ramirez, Microporous and Mesoporous Materials 128 (2010) 91.
[73] N.Audebrand, N.Guillou, J.P.Auffredic, D.Louer, Thermochimica Acta 286 (1996) 83.

[74] E.S. Els hazly, O.A.A. Abdlal, International Journal of Metallurgical Engineering 1(2012) 130.
[75] R.Von Hagen, A. Lepcha, M. Hoffman, M. Di Biasi, S.Mathur**,** Nanostructured Materials and Nanotechnology V: Ceramic Engineering 32 (2011) 3.
[76] R.H. Perry, D.W. Green, Perry's Chemical Engineers' Handbook, seventh ed., McGraw-Hill, 1997, 2571.
[77] J. Perez-Ramirez, J.C. Groen, A. Bruckner, M.S. Kumar, U. Bentrup, M.N. Debbagh, L.A. Villaescusa, J. Catal. 232 (2005) 318.
[78] Y. Li, S. Liu, Z. Zhang, S. Xie, C. Zhu, L. Xu, Appl. Catal., A, 338 (2008) 100.
[79] A. N. C. van Laak, S. L. Sagala, J. Zec˘evic´, H. Friedrich, P. E. de Jongh, K. P. de Jong, J. Catal., 276 (2010) 170.
[80] V.M. Mello, G.P.A.G. Pousa, M.S.C. Pereira, I.M. Dias, P.A.Z. Suarez, Fuel Processing Technology, 92 (2011) 53